Accurate Reactive Power Sharing Strategy for Droop-based Islanded AC Microgrids

Mohammed, Nabil; Lashab, Abderezak; Ciobotaru, Mihai; Guerrero, Josep M.

Published in:
I E E E Transactions on Industrial Electronics

DOI (link to publication from Publisher):
10.1109/TIE.2022.3167141

Publication date:
2022

Document Version
Publisher's PDF, also known as Version of record

Accurate Reactive Power Sharing Strategy for Droop-based Islanded AC Microgrids

Nabil Mohammed, *Member, IEEE*, Abderezak Lashab, *Member, IEEE*,
Mihai Ciobotaru, *Senior Member, IEEE*, and Josep M. Guerrero, *Fellow Member, IEEE*

***Abstract*—In islanded AC microgrids, the mismatched impedances of the interfacing feeders between the inverters and the load bus cause poor reactive power sharing when the conventional frequency and voltage droop control technique is employed. Such operation endangers the whole microgrid reliability as it may lead to overloading certain inverters and, consequently, triggering protection relays and causing cascaded failure. Thus, this paper proposes an accurate reactive power sharing strategy that considers the mismatched feeder impedances in islanded AC microgrids. It is based on the optimal tuning of the virtual complex impedance for each inverter. The proposed strategy has several advantages. First, it has a physical meaning as it establishes an explicit relationship between the mismatched values of the actual resistive-inductive feeders and the assigned values for the proposed virtual complex impedance to each inverter. Hence, further degradations in the microgrid voltages are prevented. Second, there is no need for prior knowledge about the actual feeder impedances in the design stage as they are estimated online from the available measurements. Lastly, the proposed control is reliable and fault-tolerant as it copes with unexpected failures such as failure of (or sudden switching off)some inverters and communication disruptions/delays. It ensures accurate power sharing even under the primary controllers after losing communication links with the secondary controller. The simulation and experimental verification results are presented to validate the performance of the proposed technique.**

***Index Terms*—Adaptive control, DC-AC power converters, impedance measurement, optimal tuning, microgrids, reactive power, virtual impedance.**

I. Introduction

THE fast growth in the global electricity demand and the need to utilize environment-friendly energy sources accelerate the advancements in the power electronics systems. As a sequence, there is a substantial annual increase in the number of distributed power generation systems (DPGSs) installed close to the load centers [1]. Additionally, clustering of small-scale generation units forms microgrids to provide reliable and optimal integration of inverter-based DPGSs, as they can be operated in the grid-connected or islanded mode [2].

N. Mohammed and M. Ciobotaru are with the School of Engineering, Macquarie University, NSW 2109, Australia (e-mail: nabil.mohammed@ieee.org; ciomih@ieee.org). (*Corresponding author: Nabil Mohammed*)

A. Lashab and J. M. Guerreroare are with the AAU Energy, Aalborg University, Aalborg 9220, Denmark (e-mail: abl@energy.aau.dk; joz@energy.aau.dk).

The conventional frequency and voltage droop control technique is widely used to control the islanded microgrids. This control approach of the DPGSs mimics the operation of synchronous generators. The droop characteristics are utilized to self-regulate the DPGSs output powers [3]. The conventional droop control approach approximates the line impedance to be purely inductive. However, this is not the case in resistive low voltage microgrids. [4].

While the conventional droop control can achieve proper active power sharing, it has severe limitations related to the reactive power sharing [5] in low voltage islanded microgrids. This is mainly due to the mismatched feeder impedances and the differences in the design parameters of the inverters. In microgrids, the detrimental effects of the mismatched feeder impedances on the reactive power sharing remain a major problem. For example, the inaccurate power sharing between parallel-connected inverters poses instability problems due to circulating current within the microgrid's inverters [6]. Such operation endangers reliability as it can overload certain inverters, consequently triggering overloading protection that may cause cascaded failure in the microgrid.

Among many suggested methods which aim to enhance the reactive power sharing in islanded microgrids, the virtual output impedance approach has gained significant popularity due to its simple implementation [7]. This technique relies on reshaping the characteristics of the inverter output impedance by establishing an additional control loop. Therefore, the coupling between the active and reactive power flow is minimized. Consequently, the reactive power sharing accuracy is improved even under mismatched feeder impedances [8].

Various studies in the literature have proposed different virtual impedance approaches. This includes designing and implementing virtual inductive [8], virtual resistive [9], and virtual complex impedance. Moreover, the virtual complex impedance is divided further into virtual resistive-inductive impedance [7], [10] and virtual resistive-capacitive impedance [11]. Even though there is substantial work available in the literature to address the reactive power sharing using the virtual impedance approach, the procedure of assigning optimal values to the virtual impedance for each inverter has not been thoroughly investigated. On the one hand, some studies recommend setting fixed values of the virtual impedances for all inverters much larger than the maximum value of line impedance expected [9]. However, this approach is impractical as good power sharing is accomplished at the expense of voltage degradation in the microgrid. Another approach is to

assign fixed values for the virtual impedances based on the summation approach [12]. It relies on setting the value of the virtual impedance of one inverter to zero while a specific value is assigned to the virtual impedance of the second inverter [12]. While the summation approach improves the reactive power sharing, it fails to regulate the errors in power sharing to zero. Furthermore, the information of the feeder impedances is assumed to be known [12].

The idea of adaptive virtual impedance has gained more attention recently [8], [13], [14]. In this approach, the value assigned to the virtual impedance is adaptively varied to improve the reactive power sharing. In [8], the virtual output impedance is implemented using an adaptive high pass filter. In [13], the tuning of the adaptive virtual impedance for each unit is performed based on the received power share reference. The adaptive virtual impedance control scheme based on small-AC-signal injection is proposed [14]. Despite the available improvements in the reactive power sharing, the major shortcomings of the existing adaptive virtual impedance methods include 1) the complex implementation, 2) the good reactive power sharing is obtained at the cost of voltage regulation in the microgrid, 3) the continuous dependence on the reliability of the communication network, and 4) most importantly, the works mentioned above have not established an explicit relation between the assigned values to the adaptive virtual impedances and the mismatched values in the physical feeder impedances, which are the cause of the inaccurate reactive power sharing phenomena in the microgrids.

This paper aims to extend the previous work [15], where further analysis, a generalized methodology, simulation results, and HIL experimental validation are considered. The proposed strategy ensures accurate reactive load power sharing between the inverters operating in islanded AC microgrids. It relies on the optimal tuning of the virtual impedances for all inverters based on the estimated feeder impedances. Hence, the main merits of this methodology include the following aspects:

1) An optimal tuning approach of virtual complex impedance for each inverter is proposed. It has a physical meaning as it considers the exact mismatched values in the physical feeder impedances.
2) An implementation of an online feeder impedance (both resistance and inductance) estimation algorithm in the microgrid central controller (MGCC) is presented. The estimation technique is simple; it uses the available measurements and ensures high accuracy and low computational burden.
3) Unnecessary voltage degradation in the microgrid is avoided. The voltage drops in the microgrid are reduced due to the use of the proposed optimal values of the virtual impedances.
4) The proposed method is reliable as it ensures accurate power sharing amongst inverters even in extreme operating conditions such as communication-link failure and sudden losing/turning off/on some inverters units. So, it supports plug and play feature.

The rest of this paper is structured as follows: Section II reviews the conventional droop control, the reactive power sharing, and the virtual impedance for islanded AC microgrids. Section III illustrates the proposed virtual impedance control scheme. Section IV and Section V present the simulation and experimental verification results. Finally, conclusions are given in Section VI.

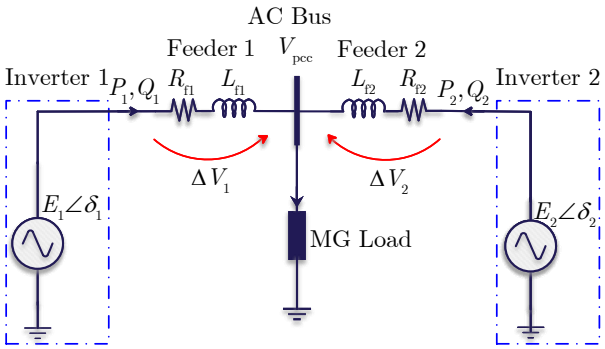

Fig. 1: Equivalent model of the islanded microgrid system consisting of two droop-based inverters.

II. Fundamental Operation Concepts of Islanded Microgrids

A. Conventional Frequency Droop Control

Fig. 1 depicts the equivalent model of an islanded microgrid that consists of two single-phase inverters and a resistive-inductive load. $E_j\angle\delta_j$ (j=1,2) represents the output voltage of DG j. $V_{pcc}\angle\theta_{pcc}$ is the microgrid voltage. Z_{f1} and Z_{f2} are the impedance of feeder 1 and feeder 2, respectively. R_{f1}, R_{f2}, X_{f1} and X_{f2} represent the resistances and reactances of the feeders.

The output active power and reactive power of the j^{th} inverter is expressed as [4]

$$P_j = \frac{X_{fj}(E_j V_{pcc}\cos\delta_j - V_{pcc}^2) + R_{fj}E_j V_{pcc}\sin\delta_j}{R_{fj}^2 + X_{fj}^2}, \quad (1a)$$

$$Q_j = \frac{X_{fj}(E_j V_{pcc}\cos\delta_j - V_{pcc}^2) - R_{fi}E_j V_{pcc}\sin\delta_j}{R_{fj}^2 + X_{fj}^2}. \quad (1b)$$

Corresponding to the small power angle δ_j: it valid to assume $\sin\delta_j \approx \delta_j$ and $\cos\delta_j \approx 1$. Furthermore, when the conventional droop assumes the feeder impedance is purely inductive, 90°, (1a) and (1b) can be reduced to

$$P_j = \frac{E_j V_{pcc}}{X_{fj}}\delta_j, \quad (2a)$$

$$Q_j = \frac{V_{pcc}(E_j - V_{pcc})}{X_{fj}}. \quad (2b)$$

It is worth mentioning that assuming feeder impedances are purely inductive is unrealistic as microgrids feeders will have non-negligible resistance [16]. Hence, the inaccurate reactive power sharing is considered an inherent drawback of the conventional droop control technique, and vice versa with active power sharing if the microgrids feeders are assumed purely resistive.

As can be seen from the assumption made in (2a) and (2b), the output active P_j and reactive Q_j power of the j^{th} inverter

can be controlled by δ_{j} and E_{j}, respectively. This goal is achieved through adjusting the frequency and the amplitude of the voltage reference provided to the outer voltage control loop by the conventional droop control as follows [3], [6]:

$$\omega_{\mathrm{j}} = \omega^* - D_p P_{\mathrm{j}}, \tag{3a}$$

$$E_{\mathrm{j}} = E^* - D_q Q_{\mathrm{j}}, \tag{3b}$$

where ω^* and E^* are the rated values of angular frequency and voltage amplitude, respectively. D_p and D_q are the droop coefficients considering the inverter capability of supplying and absorbing reactive power. These droop coefficients are calculated from the acceptable deviation limits of the frequency ($f_{\max}$, $f_{\min}$) and voltage ($V_{\max}$, $V_{\min}$) in the microgrids [6], [17].

B. Reactive Power Sharing Considering Mismatched Feeder Impedances

Even though the conventional droop ensures accurate active power sharing in the microgrids under inductive feeder impedance assumption, circulating and inaccurate reactive power between the inverters in case of unequal feeder impedances are the main challenges in such a system as will be shown below [3], [6], [8].

To simplify the analysis, the equivalent model considering two identical inverters depicted in Fig. 1 is investigated. The assumption of identical inverters is justified as identical grid-forming inverters are usually found in industrial applications to interface batteries to the islanded microgrids to maintain, for example, reliable voltage and frequency regulation [18].

The voltage drop across the impedance of feeder j is approximated by [19]

$$\Delta V_{\mathrm{j}} \approx \frac{X_{\mathrm{fj}} Q_{\mathrm{j}} + R_{\mathrm{fj}} P_{\mathrm{j}}}{E^*}. \tag{4}$$

Considering the voltage drop in (4), the terminal voltages of inverters 1 and 2 are obtained by (5a) and (5b), respectively.

$$E_1 = V_{\mathrm{pcc}} + \frac{X_{\mathrm{f1}} Q_1 + R_{\mathrm{f1}} P_1}{E^*}, \tag{5a}$$

$$E_2 = V_{\mathrm{pcc}} + \frac{X_{\mathrm{f2}} Q_2 + R_{\mathrm{f2}} P_2}{E^*}. \tag{5b}$$

Now, if Z_{f1} is larger than Z_{f2}, the mismatched impedance components between the two feeders are calculated as follows:

$$\Delta R_{\mathrm{f}} = R_{\mathrm{f1}} - R_{\mathrm{f2}}, \tag{6a}$$

$$\Delta X_{\mathrm{f}} = X_{\mathrm{f1}} - X_{\mathrm{f2}}. \tag{6b}$$

By solving the obtained formulas, the reactive power sharing error (ΔQ) due to the mismatched components of feeder 1 and feeder 2 is derived as [20], [21]

$$\Delta Q = Q_2 - Q1 = f(\Delta R_{\mathrm{f}}, \Delta X_{\mathrm{f}}, P_{\mathrm{tot}}, Q_{\mathrm{tot}}), \tag{7}$$

where $P_{\mathrm{tot}} = P_1 + P_2$ and $Q_{\mathrm{tot}} = Q_1 + Q_2$ are the total active and reactive power demand.

Equation (7) indicates that the reactive power sharing error is a function of the mismatched impedance value between the two feeders. As a result, for identical grid-forming inverters, the inverter with the higher feeder impedance will supply less reactive power. In conclusion, the impact of the mismatched feeder impedances on the reactive power sharing between inverters j and $\mathrm{j}+1$ at the PCC (also at the terminal) is summarized in (8).

$$\begin{cases} Z_{\mathrm{fj}} > Z_{\mathrm{fj+1}}, \\ \Delta V_{\mathrm{j}} > \Delta V_{\mathrm{j+1}}, \\ Q_{\mathrm{pccj}} < Q_{\mathrm{pccj+1}}. \end{cases} \tag{8}$$

C. Virtual Impedance for Droop-based Controlled Microgrids

To rectify the inevitable shortcomings of the conventional droop control under mismatched feeder impedances, the virtual impedance approach ($Z_{\mathrm{v}} = R_{\mathrm{v}} + jX_{\mathrm{v}}$) is suggested to ensure inductive behavior at the line frequency [6], [8]. Its working principle relies on dropping of the reference voltage of the j^{th} inverter (v_{refj}), generated by both (3a) and (3b) and by the added errors from the secondary controller, in proportion to its output current (i_{j}) as summarized in (9).

$$v_{\mathrm{j}}^* = v_{\mathrm{refj}} - Z_{\mathrm{vj}} i_{\mathrm{j}}, \tag{9}$$

where v_{j}^* is the modified voltage reference for the outer voltage control loop. Adopting Z_{v} not only improves the accuracy of the reactive power sharing [5], [13] but also enhances the stability of the system as it effectively suppresses the circulating currents among the inverters [6].

The remaining challenge is determining the optimal value for Z_{v} to be assigned to each inverter. Unlike such approaches, this paper proposes an optimal approach to determine the virtual impedance for each inverter based on online estimation of the feeder impedances, as illustrated next.

III. Proposed Reactive Power Sharing Strategy

Fig. 2 to Fig. 4 depict the structure of the microgrid under investigation and the detailed implementation of the proposed reactive power sharing strategy that consists of two stages.

A. Online Estimation of Feeder Impedances

The first step to implement the proposed power sharing strategy is to know the actual values of the feeder impedances. To do so, various impedance estimation methods (intrusive and non-intrusive) can be utilized. The intrusive methods require the injection of additional disturbances to the network such as pulse injection [22], the PRBS [23], or the PQ variations [24]. On the other hand, the non-intrusive techniques estimate the grid impedance using the existing measurements without injecting additional disturbance to the network. The non-intrusive techniques include, for example, the recursive least squares (RLS) algorithm [25] and the Kalman filter [26].

This paper uses the RLS algorithm to estimate the feeder resistance and inductance. Compared to its nonintrusive counterparts, the RLS algorithm has a faster estimation time, low computational complexity, and it is suitable for impedance-based applications.

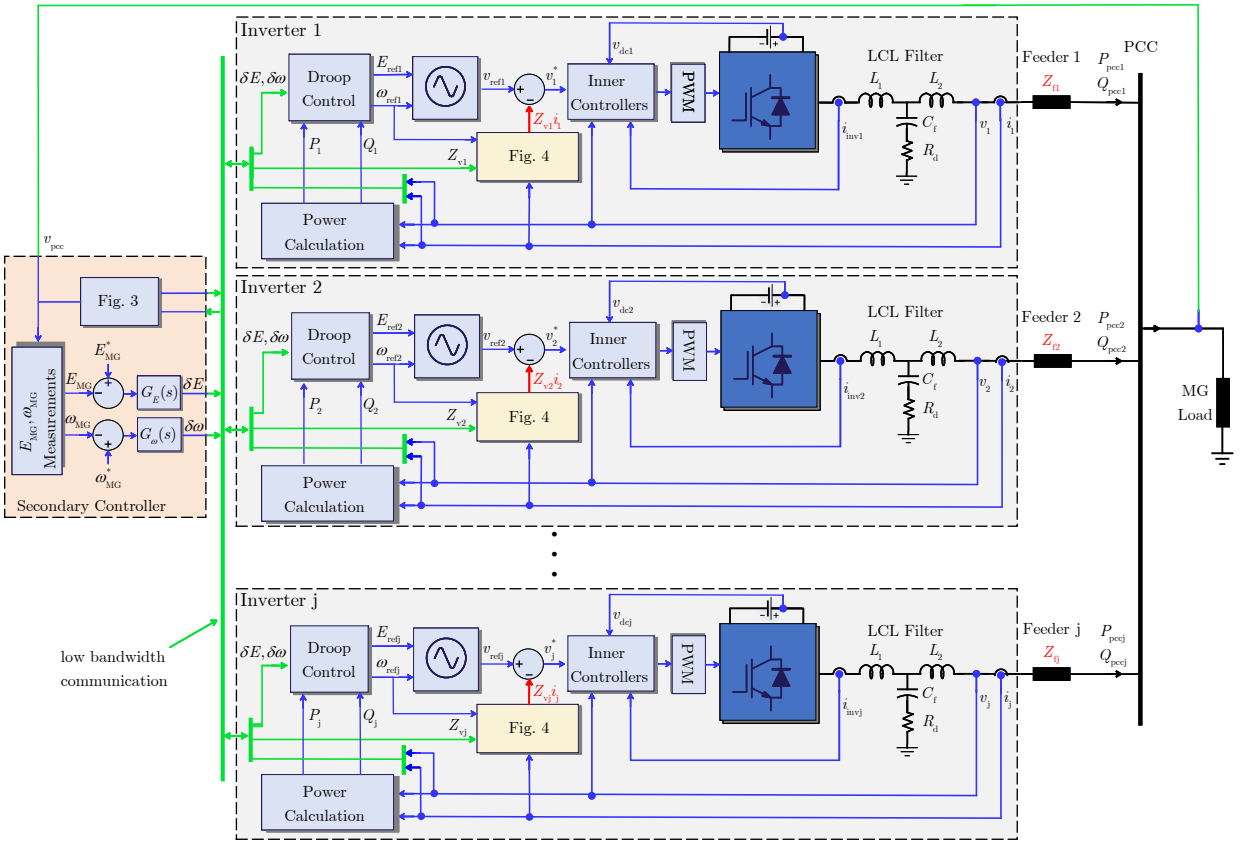

Fig. 2: A schematic diagram of the investigated islanded AC microgrid with the proposed accurate reactive power sharing strategy.

The RLS algorithm is implemented in the secondary control loop. To estimate the feeder impedance of a particular feeder, the RLS algorithm requires the current and voltage measurements at the two terminals of this feeder. For example, the impedance of feeder 1 is estimated from the i_1, v_1 and $v_{\rm pcc}$ measurements and so on.

To further elaborate, the rest of this section presents the online impedance estimation of feeder j by the j$^{\rm th}$ inverter, where j= 1,2, 3 .... Similar analysis can be followed for the online impedance estimation for other feeders.

First, the steady state operation of the j$^{\rm th}$ inverter is expressed as:

$$v_{\rm j} = R_{\rm fj} \times i_{\rm j} + L_{\rm fj} \times \frac{di_{\rm j}}{dt} + v_{\rm pcc}, \tag{10}$$

where $v_{\rm j}$ and $i_{\rm j}$ are the output voltage and current measurements of the j$^{\rm th}$ inverter, respectively. $v_{\rm pcc}$ is the common ac bus voltage.

If $v_{\rm j}$ and $v_{\rm pcc}$ are considered to be the system input variables, and $i_{\rm j}$ is the state variable, then, the continuous-time state space model of (10) is expressed as follows:

$$\begin{cases} \dot{x}(t) = \frac{di_{\rm j}}{dt} = -\frac{R_{\rm fj}}{L_{\rm fj}} i_{\rm j} - \frac{1}{L_{\rm fj}}(v_{\rm j} - v_{\rm pcc}), \\ y(t) = i_{\rm j}. \end{cases} \tag{11}$$

Eq. (11) is written in discrete-time form as shown in (12).

$$\begin{cases} x(k+1) = i_{\rm j}(k+1) = -\frac{R_{\rm fj}}{L_{\rm fj}} i_{\rm j}(k) - \frac{1}{L_{\rm fj}}(v_{\rm j}(k) - v_{\rm pcc}(k)), \\ y(k) = i_{\rm j}(k). \end{cases} \tag{12}$$

By considering the sampling interval ($T_{\rm s}$) of the measurements, the solution of the state equations shown in (12) is obtained by mapping the input and output as

$$i_{\rm j}(k) = \begin{bmatrix} i_{\rm j}(k-1) \\ v_{\rm j}(k-1) - v_{\rm pcc}(k-1) \end{bmatrix}^T \begin{bmatrix} 1 - \frac{R_{\rm fj}}{L_{\rm fj}} T_{\rm s} \\ \frac{1}{L_{\rm fj}} T_{\rm s} \end{bmatrix}. \tag{13}$$

Eq. (13) can be written in a linear regression form as:

$$y(k) = \varphi^T(k)\theta, \tag{14}$$

where $y(k)$ is the output vector that contains $i(k)$. $\varphi^T(k)$ is the input vector that consists of two variables, the delayed voltage ($v_{\rm j}(k-1)$) and current ($i_{\rm j}(k-1)$) vectors by one sample. θ is the regression vector of the unknown parameters ($R_{\rm fj}$, $L_{\rm fj}$)

The RLS algorithm can be applied now to estimate the unknown components based on the three measurement quantities ($v_{\rm j}$, $i_{\rm j}$ and $v_{\rm pcc}$).

The equations of the RLS algorithm used in the estimation are expressed in (15) at the sampling instance (k).

$$\hat{\theta}(k) = \hat{\theta}(k-1) + L(k).\varepsilon(k), \tag{15a}$$

$$\varepsilon(k) = y(k) - \varphi^T(k).\hat{\theta}(k-1), \tag{15b}$$

$$L(k) = \frac{P(k-1)\varphi(k)}{\rho + \varphi^T(k).P(k-1).\varphi(k)}, \tag{15c}$$

$$P(k) = \frac{1}{\rho}[P(k-1) - L(k).\varphi^T(k).P(k-1)], \tag{15d}$$

where, ρ is the forgetting factor with values between 0 and 1. It compromises the convergence rate and the steady-state error [27], [28].

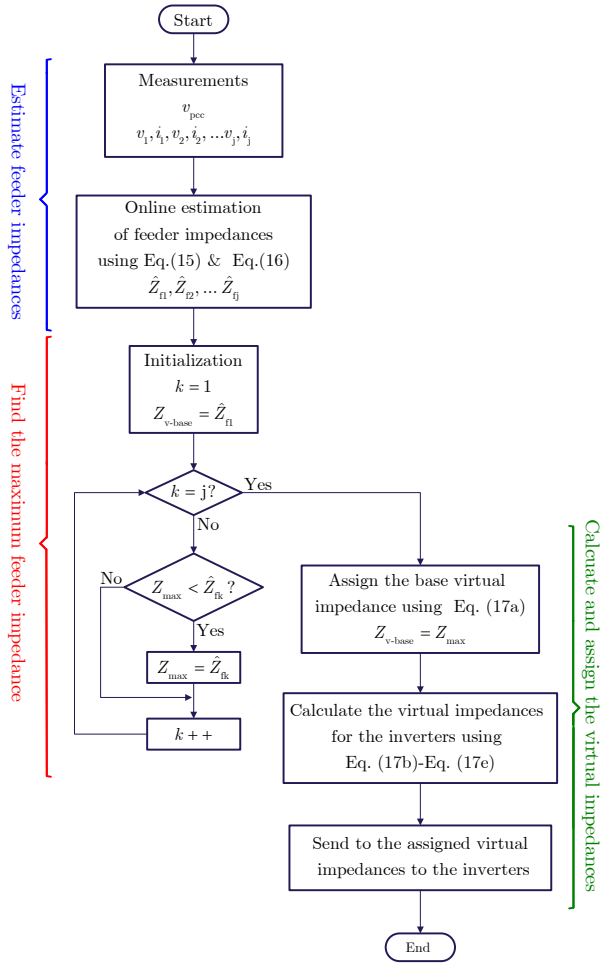

Fig. 3: Proposed algorithm to determine the optimal values of the virtual impedances for the inverters operating in the islanded AC microgrid.

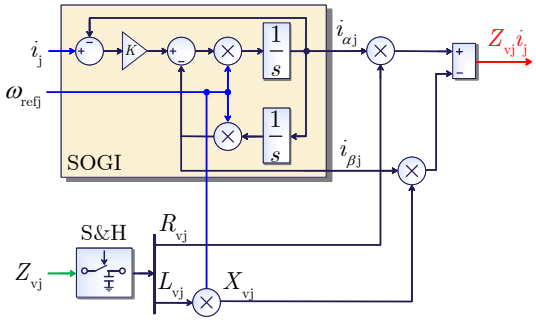

Fig. 4: Implementation of the proposed reactive power sharing strategy using the optimal virtual complex impedance, which is based on the online estimation of the feeder impedances for the jth inverter (j= 1, 2, 3, ...).

Unlike other algorithms that intend to reduce the mean square error (MSE), the RLS algorithm recursively estimates the unknown parameters that minimize the weighted linear least-squares cost function relating to the measured signals; see (15b). After a few iterations, the best fits for the unknown parameters are selected upon reaching the convergence. Finally, the resistance and inductance components of the jth feeder are calculated directly from the estimated regression vector $\hat{\theta}$ in (15) as shown below:

$$\begin{bmatrix} \hat{R}_{fj} \\ \hat{L}_{fj} \end{bmatrix} = \begin{bmatrix} (1-\hat{\theta}_1)/\hat{\theta}_2 \\ T_s/\hat{\theta}_2 \end{bmatrix}. \tag{16}$$

It is worth mentioning that the estimated feeder impedances are performed before enabling the proposed control, where the RLS algorithm is executed in the secondary control loop only for a short time (a few ten milliseconds). As the RLS algorithm utilizes remote measurements (the inverter output current and voltage) for the impedance measurement based on (15) and (16), the estimation accuracy could be impacted by possible communication delays. To minimize such delays, the sampling rate of the RLS algorithm can be set to a slow sampling rate than the sampling rate of the inverter control algorithm. Finally, the estimated impedances are saved to calculate the proposed optimal virtual impedance for each inverter, as will be explained next.

B. Implementation of the Proposed Optimal Virtual Impedance

Fig. 3. shows the methodology followed to optimally tune the virtual impedances of all inverters. The calculation of these virtual impedances is performed in the secondary control loop. The estimated feeder impedances based on (16) of all feeders (e.g., $\hat{Z}_{f1} = \hat{R}_{f1} + j\hat{X}_{f1}$, $\hat{Z}_{f2} = \hat{R}_{f2} + j\hat{X}_{f2}$, and $\hat{Z}_{fj} = \hat{R}_{fj} + j\hat{X}_{fj}$) are compared to find the highest value to be taken as the base virtual impedance, $Z_{v-base} = R_{v-base} + jX_{v-base}$, as summarized in (17a). The control laws of the proposed optimal virtual impedances Z_{v1}, Z_{v2}, ...,Z_{vj} for inverters $1, 2, ..., j$ in the microgrid shown Fig. 2 are obtained based on the difference (mismatched) between Z_{v-base} and the estimated impedances of their own feeders, as given in (17b)-(17e):

$$\begin{cases} Z_{v-base} = Z_{max} = \max(\hat{Z}_{f1}, \hat{Z}_{f2}, \hat{Z}_{f3}). & (17a) \\ Z_{v1} = (R_{v-base} - \hat{R}_{f1}) + j(X_{v-base} - \hat{X}_{f1}), & (17b) \\ Z_{v2} = (R_{v-base} - \hat{R}_{f2}) + j(X_{v-base} - \hat{X}_{f2}), & (17c) \\ \ldots, & (17d) \\ Z_{vj} = (R_{v-base} - \hat{R}_{fj}) + j(X_{v-base} - \hat{X}_{fj}), & (17e) \end{cases}$$

where R_{v1}, R_{v2}, R_{vj}, X_{v1}, X_{v2}, X_{vj} are the real and imaginary components of the proposed optimal virtual impedances for inverters 1, 2, and j, respectively.

Next, the assigned values for the virtual impedances by (17) in the secondary controller are sent to the inverters to be used in their primary control loops (9). For the jth inverter, implementing the term $Z_{vj} \times i_j$ requires the time derivative of the inverter output current, making the system highly sensitive to the output current noise. To solve this issue, the second-order generalized integrator (SOGI) approach is utilized [7]. Hence, (9) can be rewritten for the jth inverter under the proposed control as follows:

$$v_j^* = v_{refj} - (R_{vj} \times i_{\alpha j} - X_{vj} \times i_{\beta j}), \tag{18}$$

where $i_{\alpha j}$ and $i_{\beta j}$ are the two components of the inverter output current in the $\alpha\beta 0$ stationary reference frame.

The assigned optimal virtual impedances to all inverters equalize the voltage drop across these feeders of the microgrid. As a result, the negative impacts of the mismatched feeder impedances on the reactive power sharing are fully mitigated. In other words, the performance of the reactive power sharing after enabling the proposed control strategy can be summarized as follows:

$$\begin{cases} (Z_{\rm f1}+Z_{\rm v1})i_1=(Z_{\rm f2}+Z_{\rm v2})i_2=...=(Z_{\rm fj}+Z_{\rm vj})i_{\rm j}, \\ \Delta V_1=\Delta V_2=...=\Delta V_{\rm j}, \\ Q_1=Q_2=...=Q_{\rm j}, \end{cases} \tag{19}$$

where Q_1, Q_2 and $Q_{\rm j}$ are the injected reactive power by inverter 1, inverter 2 and inverter j, respectively.

It is worth mentioning that while other design approaches in (17) could be adopted, only the proposed approach of fixing the base virtual impedance to the originally maximum feeder impedance ensures the optimal solution. Simultaneously with achieving 100% accurate reactive power sharing among the inverters, it prevents unnecessary voltage drops in the microgrid even after communication link failure as the virtual impedance of each inverter is required to be initialized only for one time regardless of the load changes. Hence, after losing the communication between the secondary control and primary control layers, the proposed control strategy continues to ensure the accurate reactive power sharing by using the virtual impedance sent earlier from the secondary control loop.

C. Stability Analysis

This paper analyzes only the stability of Fig. 5, as it is the main part of the proposed scheme. As stated earlier, the SOGI is used to implement the proposed virtual impedance for each inverter, as shown in Fig. 4. It is used to obtain both the alpha and beta components of the output current of the j$^{\rm th}$ inverter. The SOGI closed-loop transfer functions for alpha and beta channels are given by (20) and (21), respectively [29].

$$G_\alpha(s)=\frac{K\omega_{\rm refj}s}{s^2+K\omega_{\rm refj}s+\omega_{\rm refj}^2}, \tag{20}$$

$$G_\beta(s)=\frac{K\omega_{\rm refj}^2}{s^2+K\omega_{\rm refj}s+\omega_{\rm refj}^2}, \tag{21}$$

where K is the gain of the SOGI closed-loop transfer functions. It is set to 0.35 in this paper to compromise between the time response and the bandwidth of the filter [7], [29]. $\omega_{\rm refj}$ is the angular frequency reference of the j$^{\rm th}$ inverter.

The closed-loop transfer function of the proposed control (the SOGI and the virtual impedance) for the j$^{\rm th}$ inverter shown in Fig. 4 is given as follows:

$$G_{\rm vj}(s)=K\omega_{\rm refj}s\times\frac{\omega_{\rm refj}R_{\rm vj}-{\omega_{\rm refj}}^2L_{\rm vj}}{s^2+K\omega_{\rm refj}s+\omega_{\rm refj}^2}; \tag{22}$$

Considering the transfer function $G_{\rm v}(s)$ in (22) and the parameters listed in Table I, the Bode plot and root locus of the system are plotted in Fig. 6(a) and Fig. 6(b), respectively. It can be noticed from Fig. 6(a) that the proposed combination of the SOGI and the optimal virtual impedance approach operates

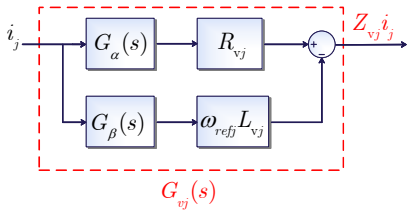

Fig. 5: Simplified control block diagram of Fig. 4 that is being used for implementing the proposed virtual impedance for the j$^{\rm th}$ inverter.

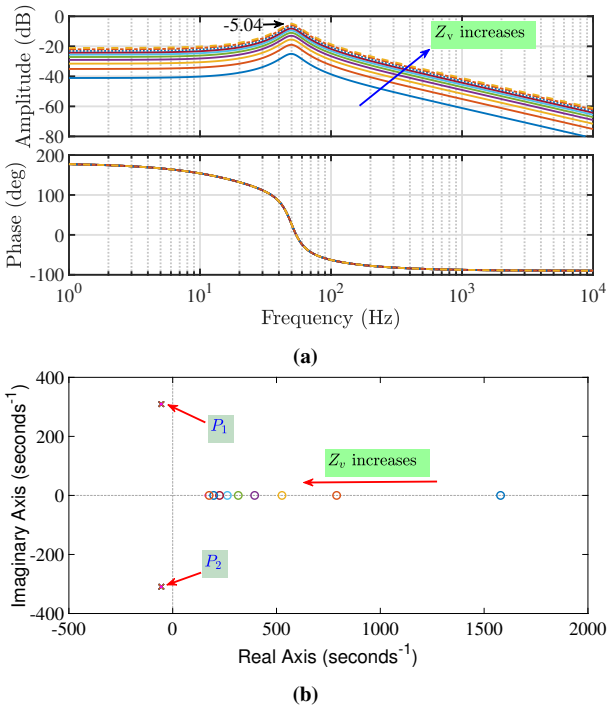

Fig. 6: (a) Bode plot, (b) Root locus of transfer function of the proposed virtual impedance control loop, where K = 0.35, $\omega_{\rm refj}$ = $2\pi50$ rad/sec, and $Z_{\rm vj}$ increases from 0.1+0.08s, to 0.5+0.8s.

mainly at the fundamental frequency to effectively modify the output impedance of the inverter in order to ensure the accurate reactive power sharing. $Z_{\rm v}$ behaves as a low pass filter (LPF) after the system frequency 50 Hz with a magnitude slope of -20 dB/dec. The root locus of the transfer function $G_{\rm v}(s)$ shown in Fig. 6(b) indicates that increasing $Z_{\rm v}$ leads to moving the zeros closer towards the origin while the system two poles are kept constant and far from the imaginary axis.

IV. Simulation Results

To demonstrate the efficacy of the proposed control strategy, the islanded AC microgrid shown in Fig. 2 is considered. The system is simulated in MATLAB/Simulink software. Table. I lists the system parameters used in the simulation.

A. Power Sharing Under Identical Power Ratings

To obtain the key simulation results, the performance of the system is tested under different conditions as follows:

1) Test 1 (t < 3 sec): the system operation under the conventional control is examined for a microgrid load equal to $P_{\rm load}$= 3 kW and $Q_{\rm load}$= 3 kVar.

TABLE I: The parameters of the islanded AC microgrid.

Quantity	Symbol	Value	Unit
Microgrid parameters			
Nominal voltage (Max)	E^*_{MG}	230 $\sqrt{2}$	V
Nominal frequency	ω^*_{MG}	2π 50	rad/sec
load power	P^*_{Load}	3 & 6	kW
	Q^*_{Load}	3 & 6	kVar
Impedance of feeder 1	R_{f1}	1	Ω
	L_{f1}	1.6	mH
Impedance of feeder 2	R_{f2}	0.5	Ω
	L_{f2}	0.8	mH
Impedance of feeder 3	R_{f3}	0.75	Ω
	L_{f3}	1.2	mH
DG1 and DG2 parameters			
Inverter nominal power	P_n	5	kW
Inverter nominal current (RMS)	I_n	21.74	A
Primary controller			
Frequency droop gain	m_p	0.0013	rad/sec/W
Voltage droop gain	n_p	0.0052	V/Var
Secondary controller			
Frequency restoration gains	$K_{p-\omega}$	1	-
	$K_{i-\omega}$	10	1/sec
Voltage restoration gains	K_{p-E}	1	-
	K_{i-E}	100	1/sec

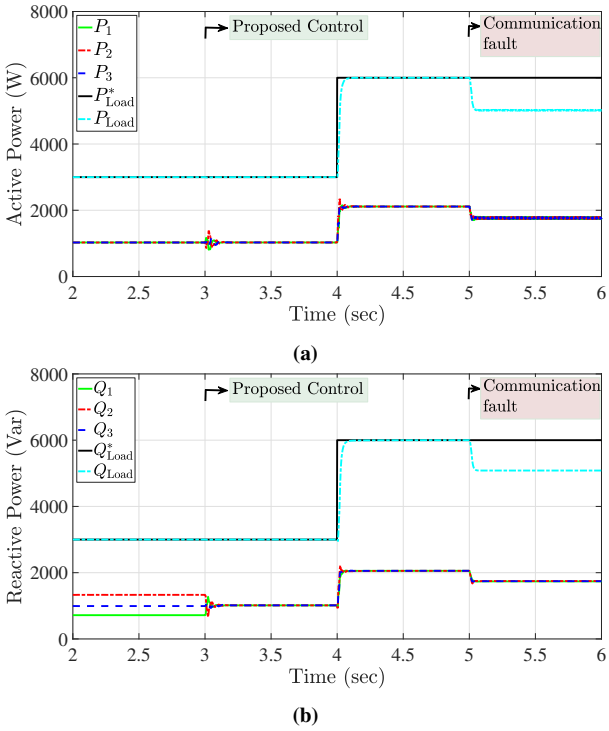

Fig. 7: The simulation results of the power sharing in the microgrid: (a) active power, and (b) reactive power.

2) Test 2 ($t = 3$ sec): the proposed control is enabled, where the virtual impedances of inverters 1, 2, and 3 are set according to (17).
3) Test 3 ($t = 4$ sec): a step change in the microgrid load to P_{load}= 6 kW and to Q_{load}= 6 kVar is applied under the proposed control.
4) Test 4 ($t = 5$ sec): a failure in the communication links between the secondary controller and the inverters is tested.

Fig. 7(a) and Fig. 7(b) show the active and reactive power of the microgrids. It can be seen that the delivered powers to the load track perfectly the references as long as the secondary controller is enabled. Furthermore, regardless of the mismatch impedances of the feeders, the active load is shared equally between the three inverters, 1 kW each for $t < 4$ sec and 2 kW each for $t \geq 4$ sec. However, the reactive load power is not shared accurately by the three inverters under the conventional droop control. For example, the injected reactive power by the 1^{st} inverter is equal to Q_1= 0.75 kW while Q_2= 1.25 kW, where $Z_{\text{f1}} > Z_{\text{f2}}$; see (8).

Fig. 7(b) shows that the errors in the reactive power sharing are remarkably reduced, and the three inverters share the same amount of reactive power under the proposed control scheme for $t \geq 4$ sec. For instance, the delivered power to the PCC by each inverter is equal to 1 kVar for 3-4 sec and 2 kVar for 4-5 sec. Fig. 7 shows the system response remains stable after enabling the virtual impedances at t = 3 sec. This finding of stable operation is predicted by the stability analysis shown in Fig. 6(b) in which the closed-loop transfer function of the added virtual impedance loop has two poles (P_1 and P_2) located in the left hand side of the s-plane. Hence,

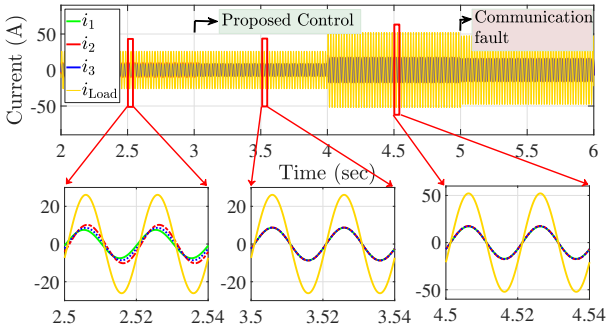

Fig. 8: The microgrid current waveforms.

it can be seen that the reactive power sharing manifests an excellent dynamic performance and no instability phenomenon has occurred.

Fig. 8 depicts the current waveforms in the microgrid. The magnitudes and phase of current waveforms are not identical under the traditional droop control. In contrast, the current waveforms of the three inverters have identical magnitude and phase after enabling the proposed control for $t \geq 3$ sec.

Fig. 9 presents the online estimation results of the feeder resistance and inductance by inverter 1. It can be observed that the RLS algorithm provides very accurate estimation results after it is enabled for t >= 3 sec. Note that the accuracy of impedance estimation mainly relies on the forgotten factor parameter of the RLS algorithm. In this paper, this parameter is set to 0.995 to provide the accurate and stable estimation.

Fig. 10 shows the amplitudes of voltage references provided by droop control of each inverter. Under the traditional control, the highest voltage reference value is for inverter 1 as the

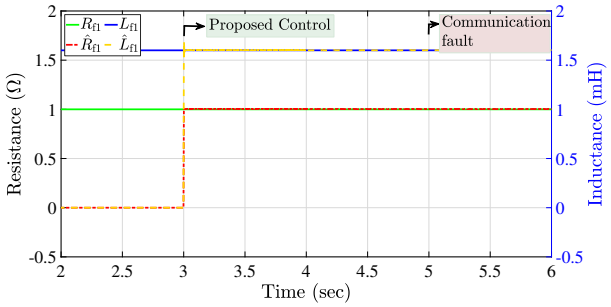

Fig. 9: The online impedance estimation of feeder 1.

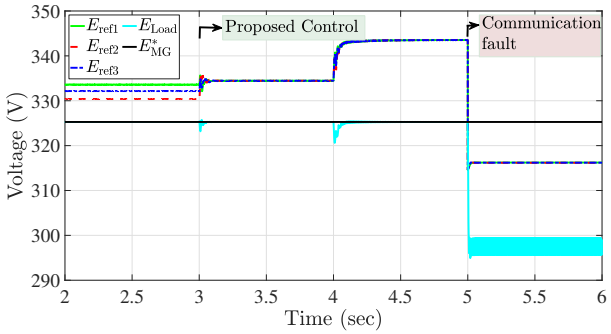

Fig. 10: The voltages magnitudes of the inverters and the microgrid load.

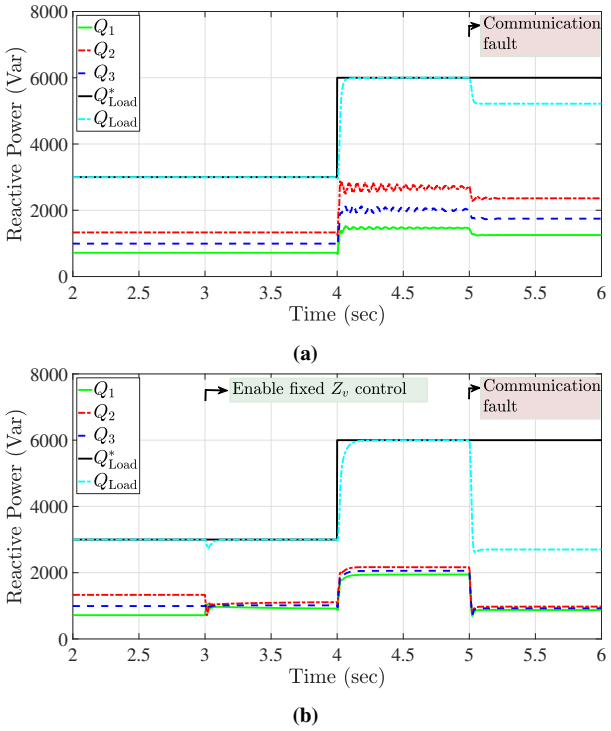

Fig. 11: Comparison of the proposed reactive load power sharing technique, shown in Fig. 7(b), with: (a) Conventional control without virtual impedances (Z_{v2}=Z_{v1}=Z_{v3}=0), (b) Conventional control with fixed virtual impedances for all inverters (R_{vj}= $7R_{v1}$ Ω), and L_{vj}= $7L_{v1}$ mH).

impedance of its feeder has the largest value. The differences in these voltages are compensated completely after enabling the proposed control. Fig. 10 also shows the voltage amplitude of the microgrid load and its reference. It can be seen that, before the communication fault, the secondary control loop regulates the microgrid voltage to its nominal value of $230\sqrt{2}$ V.

B. Comparison With Conventional Methods

As the available literature does not utilize the online estimation of the feeder impedances to tune the virtual impedances, the performance is compared in this paper against two conventional methods, where there is no virtual impedance and with a fixed virtual impedance scheme. These two methods are considered base case studies in the literature. Similar to the proposed method, these two methods are implemented in the centralized microgrid.

Fig. 11(a) and Fig. 11(b) provide the reactive load power sharing results obtained with no virtual impedance and a fixed virtual impedance scheme, respectively. Both control schemes fail to achieve zero steady-state errors in the reactive power sharing between the identical inverters due to the mismatched feeder impedances. Hence, the proposed control shown earlier in Fig. 7(b) outperforms these two power sharing techniques.

C. Power Sharing Under Different Power Ratings

Unlike the other cases presented in this paper, this section investigates a special case that considers the reactive power sharing between non-identical inverters with different power ratings. Two inverters are considered with 5 kW and 2.5 kW rating power, respectively. The impedance components of feeders 1 and 2 are identical to those listed in Table. I. The only difference in this case study is the tuning procedure of the virtual impedances. Considering the difference in the power ratings, the injected power by inverter 1 in the ideal operation should be double the injected power by inverter 2. Hence, to achieve accurate reactive power sharing through equal voltage droop across the feeders, Z_v of inverter 2 is taken double to its value calculated by (17).

Fig. 12 shows the reactive load power sharing among inverters 1 and 2. The conventional control (t <3 sec) not only fails to ensure the proportional reactive power sharing, but also the inverter with the lower power rating (inverter 2) supplies reactive power more than the inverter with the higher power rating (inverter 1). For t >3 sec, fair sharing of the load reactive power among the two inverters is achieved concerning their power rating differences.

D. Performance During Faults in the System

Fig. 13 presents the reactive power sharing for four different scenarios: normal operation before t= 5 sec, communication fault at t=5 sec, switching off inverter 1 (DG1) at t=6 sec, and load change at $t \geq 7$ sec. In these scenarios, the proposed control validates to be reliable as it ensures the accurate active and reactive power sharing among the inverters. For instance, after losing inverter 1 at 6 sec, the load power is distributed equally between inverters 2 and 3. Furthermore, the control strategy copes with the sudden load change at 7 sec while communication is unavailable. This validates the robustness of

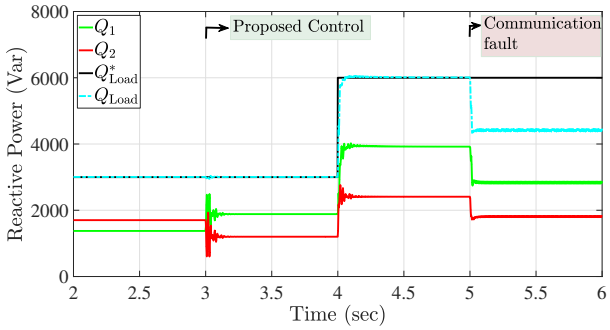

Fig. 12: Reactive power sharing between two non-identical inverters under the proposed power sharing technique, $P_{n1} = 2P_{n2}$= 5 kW.

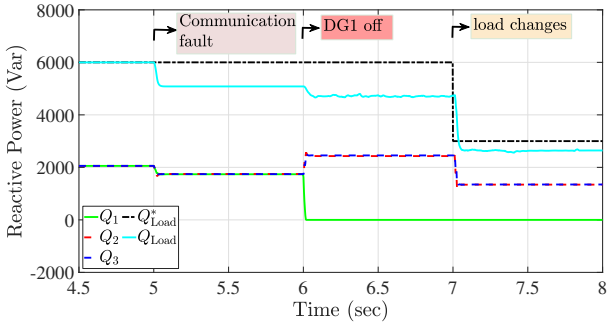

Fig. 13: Reactive load power sharing in the microgrid under abnormal operation: communication failures at 5 sec, switching off DG1 at 6 sec, and load change while communication is unavailable at 7 sec.

the proposed reactive power sharing against various abnormal operating conditions.

V. Hardware-in-the-loop Experimental Results

To further verify the power sharing performance of the proposed strategy, hardware-in-the-loop (HIL) experiments are conducted on a single-phase ac microgrid with two DG units, as depicted in Fig. 14. The power stage (electric part of the circuit) is emulated using PLECS RT Box. The control algorithm is realized through a TMS320F28069M LaunchPad from Texas Instruments. The parameters chosen for the HIL test bench are identical to those used for the simulation, as listed in Table. I.

This section has tested three different cases under the mismatch in the impedances of feeders 1 and 2. In case 1, the power sharing between the two inverters is investigated when supplying a common resistive-inductive microgrid load. Then, case 2 considers only a resistive load to verify the performance improvement by eliminating the circulating reactive power between the two inverters. In case 3, the performance of the proposed control is tested for the loss of communication links between the secondary controller and the two inverters.

A. Active and Reactive Load Power Sharing

In this case, the power rating of each inverter is 5 kW. Hence, it is expected that the load power to be proportionally and equally shared among the two parallel inverters. The power sharing of the initial 3 kW and 3 kVar microgrid load is shown in Fig. 15(a) and Fig. 15(b), respectively. Initially,

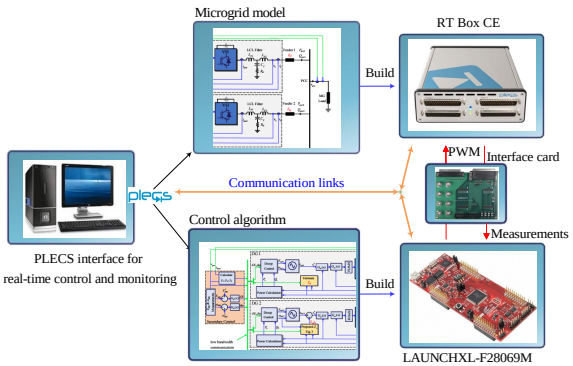

(a)

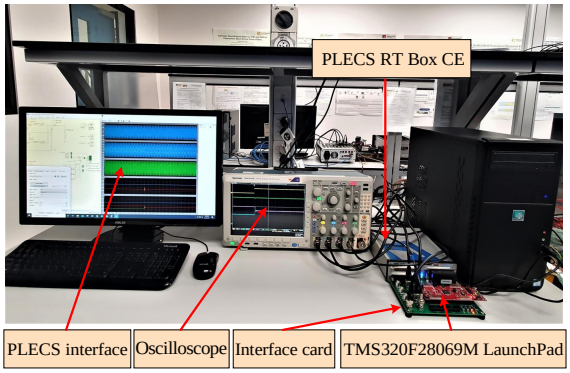

(b)

Fig. 14: Hardware-in-the-loop setup: (a) Block diagram of the setup, (b) Screenshot of the setup.

the reactive load power sharing is poor under the conventional control strategy. As a sequence, the output current waveforms of the two inverters are significantly different from each other, as shown in Fig. 15(c).

When the proposed control strategy is enabled, the output currents of the inverters are gradually equalized. Fig. 15(a) and Fig. 15(b) also show that the proposed control strategy ensures the proportional and equal reactive power sharing after the load change to 6 kW and 6 kVar at t_1.

B. Eliminating the Circulating Reactive Power Between Inverters

The microgrid load is set to 3 kW. Then, the efficacy of the proposed control strategy under different impedances for feeders 1 and 2 is tested. Fig. 16(a) and Fig. 16(b) show the obtained results. While the inverters supply the same amount of active power to the load under the conventional control, the circulating reactive power between the inverters caused by the mismatched impedances is relatively large; see Fig. 16(a). After enabling the proposed control strategy that compensates adaptively for the mismatched voltage drops, the output currents of both inverters become almost identical.

C. Loss of Communication Links

Fig. 17(a) and Fig. 17(b) verify the reliability of the proposed power sharing strategy against a failure in the communication links in the microgrid at t_1. The reactive power

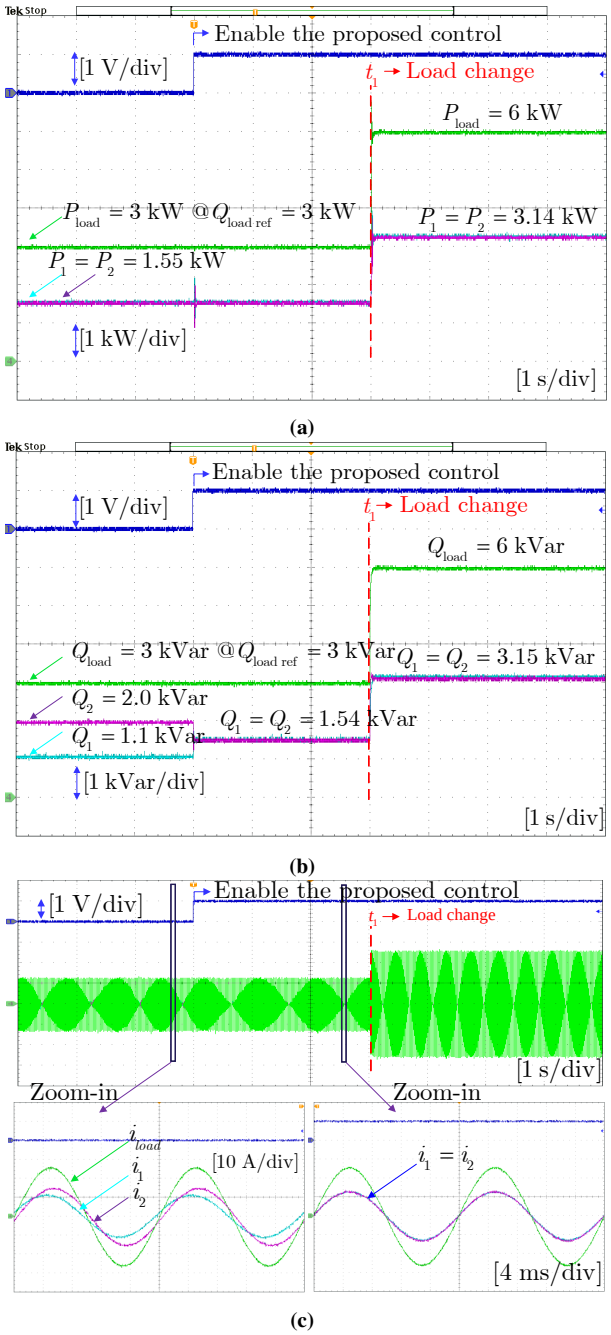

Fig. 15: The experimental results of the power sharing under the conventional and the proposed control: (a) Active power, (b) Reactive power, (c) current waveforms.

sharing between the two inverters is maintained accurately after t_1.

The superiority of the proposed control accurate reactive power sharing over three existing techniques is summarized in Tab. II. It can be observed that the proposed method has several advantages that include achieving very accurate reactive power sharing under abnormal conditions such as communication faults and load, whereas other methods fail in such operational scenarios.

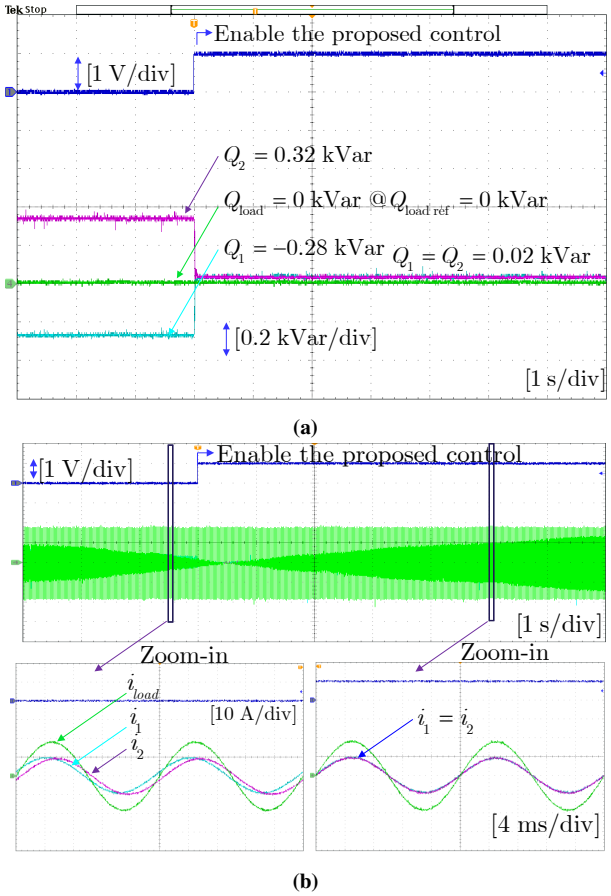

Fig. 16: Experimental results of under the conventional and the proposed control: (a) Circulating reactive power, (b) Current waveforms.

VI. Conclusions

In this paper, a power sharing strategy scheme is proposed to enhance the accuracy of reactive power sharing in islanded AC microgrids. The control strategy deploys the online estimation of the feeder impedances for optimal tuning of the complex virtual impedance assigned to each inverter. The followed control approach provides an effective mechanism for real and reactive power decoupling. Hence, despite mismatched feeder impedances, proportional load sharing among parallel-connected inverters is achieved. Additionally, the voltage degradation in the microgrid load is avoided due to: 1) optimizing the value of the proposed virtual impedances; and 2) deploying the secondary control level. Finally, the simulation and HIL experiment results validate the effectiveness of the proposed scheme.

Several important aspects can be considered in future studies. First, microgrids with multiple PCCs and different typologies (e.g., meshed microgrids, interconnected DC and AC microgrid clusters) can be investigated. Second, future studies can also consider non-identical inverters, including the aging factor that could cause asymmetrically degradation of the components among different inverters.

References

[1] F. Blaabjerg, R. Teodorescu, M. Liserre, and A. V. Timbus, "Overview of control and grid synchronization for distributed power generation

TABLE II: Comparison between the proposed reactive power sharing strategy and different virtual-based impedance techniques.

Ref	Strategy	Consider mismatch feeder impedances?	Reactive sharing Accuracy	MG voltage degradation	Require communication/ Robustness against faults	Control Complexity
[6]	Fixed Z_v for all inverters	No	Low	Large	no communication	low
[13]	Unique Z_v for each inverter	Yes	High	Minimal	Yes/good	high
[30]	Consensus-based virtual impedance	Yes	depends on optimization	-	Yes/poor	high
[Proposed]	Unique Z_v for each inverter	Yes	High	Minimal	Yes/very well	medium

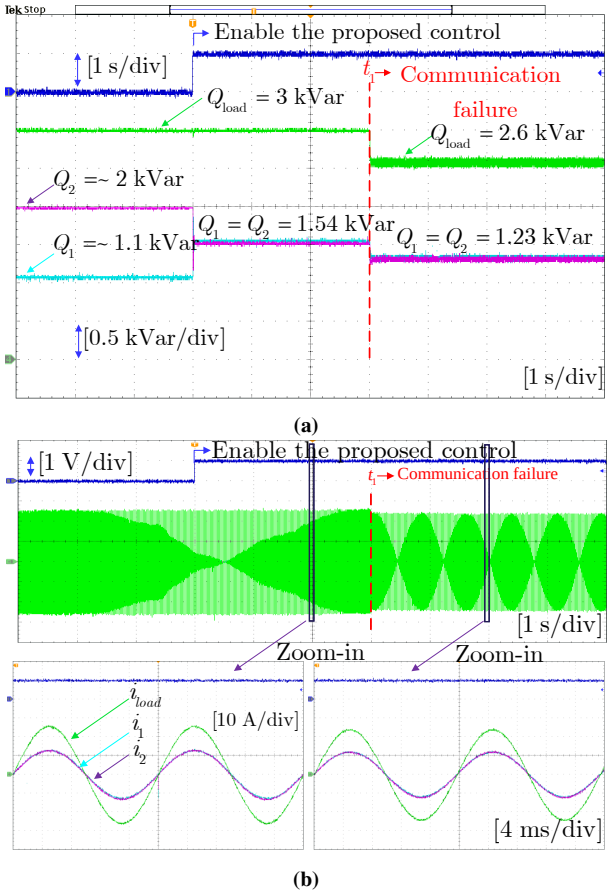

Fig. 17: Experimental results of the reactive power under a communication link failure: (a) Reactive power, (b) Current waveforms.

systems," *IEEE Trans. Ind. Electron.*, vol. 53, no. 5, pp. 1398–1409, 2006.

[2] H. Jiayi, J. Chuanwen, and X. Rong, "A review on distributed energy resources and MicroGrid," *Renew. Sust. Energ.*, vol. 12, no. 9, pp. 2472–2483, 2008.

[3] M. C. Chandorkar, D. M. Divan, and R. Adapa, "Control of parallel connected inverters in standalone AC supply systems," *IEEE Trans. Ind. Appl.*, vol. 29, no. 1, pp. 136–143, 1993.

[4] Y. Han, H. Li, P. Shen, E. A. A. Coelho, and J. M. Guerrero, "Review of active and reactive power sharing strategies in hierarchical controlled microgrids," vol. 32, no. 3, pp. 2427–2451, 2016.

[5] U. B. Tayab, M. A. B. Roslan, L. J. Hwai, and M. Kashif, "A review of droop control techniques for microgrid," *Renew. Sust. Energ.*, vol. 76, pp. 717–727, 2017.

[6] J. M. Guerrero, J. C. Vasquez, J. Matas, L. G. De Vicuña, and M. Castilla, "Hierarchical control of droop-controlled AC and DC microgrids—A general approach toward standardization," *IEEE Trans. Ind. Electron.*, vol. 58, no. 1, pp. 158–172, 2010.

[7] J. Matas, M. Castilla, L. G. De Vicuña, J. Miret, and J. C. Vasquez, "Virtual impedance loop for droop-controlled single-phase parallel inverters using a second-order general-integrator scheme," vol. 25, no. 12, pp. 2993–3002, 2010.

[8] J. M. Guerrero, L. G. De Vicuna, J. Matas, M. Castilla, and J. Miret, "Output impedance design of parallel-connected UPS inverters with wireless load-sharing control," *IEEE Trans. Ind. Electron.*, vol. 52, no. 4, pp. 1126–1135, 2005.

[9] J. M. Guerrero, J. Matas, L. G. de Vicuna, M. Castilla, and J. Miret, "Decentralized control for parallel operation of distributed generation inverters using resistive output impedance," *IEEE Trans. Ind. Electron.*, vol. 54, no. 2, pp. 994–1004, 2007.

[10] W. Yao, M. Chen, J. Matas, J. M. Guerrero, and Z.-M. Qian, "Design and analysis of the droop control method for parallel inverters considering the impact of the complex impedance on the power sharing," *IEEE Trans. Ind. Electron.*, vol. 58, no. 2, pp. 576–588, 2010.

[11] A. Micallef, M. Apap, C. Spiteri-Staines, J. M. Guerrero, and J. C. Vasquez, "Reactive power sharing and voltage harmonic distortion compensation of droop controlled single phase islanded microgrids," vol. 5, no. 3, pp. 1149–1158, 2014.

[12] C. N. Rowe, T. J. Summers, R. E. Betz, T. G. Moore, and C. D. Townsend, "Implementing the virtual output impedance concept in a three phase system utilising cascaded PI controllers in the dq rotating reference frame for microgrid inverter control," in *2013 15th European Conference on Power Electronics and Applications (EPE)*. IEEE, 2013, pp. 1–10.

[13] H. Mahmood, D. Michaelson, and J. Jiang, "Accurate reactive power sharing in an islanded microgrid using adaptive virtual impedances," vol. 30, no. 3, pp. 1605–1617, 2014.

[14] B. Liu, Z. Liu, J. Liu, R. An, H. Zheng, and Y. Shi, "An adaptive virtual impedance control scheme based on small-AC-signal injection for unbalanced and harmonic power sharing in islanded microgrids," vol. 34, no. 12, pp. 12 333–12 355, 2019.

[15] N. Mohammed and M. Ciobotaru, "An Accurate Reactive Power Sharing Strategy for an Islanded Microgrid Based on Online Feeder Impedance Estimation," in *IECON 2020 The 46th Annual Conference of the IEEE Industrial Electronics Society*. IEEE, 2020, pp. 2525–2530.

[16] J. Rocabert, A. Luna, F. Blaabjerg, and P. Rodriguez, "Control of power converters in AC microgrids," *IEEE transactions on power electronics*, vol. 27, no. 11, pp. 4734–4749, 2012.

[17] M. S. Rahman, M. Hossain, and J. Lu, "Coordinated control of three-phase AC and DC type EV–ESSs for efficient hybrid microgrid operations," *Energy conversion and management*, vol. 122, pp. 488–503, 2016.

[18] M. Hossain, H. Pota, A. Haruni, and M. Hossain, "DC-link voltage regulation of inverters to enhance microgrid stability during network contingencies," *Electric Power Systems Research*, vol. 147, pp. 233–244, 2017.

[19] Y. W. Li and C.-N. Kao, "An accurate power control strategy for power-electronics-interfaced distributed generation units operating in a low-voltage multibus microgrid," vol. 24, no. 12, pp. 2977–2988, 2009.

[20] J. He and Y. W. Li, "An enhanced microgrid load demand sharing strategy," vol. 27, no. 9, pp. 3984–3995, 2012.

[21] H. Sellamna, A. M. Pavan, A. Mellit, and J. M. Guerrero, "An iterative adaptive virtual impedance loop for reactive power sharing in islanded meshed microgrids," *Sustainable Energy, Grids and Networks*, vol. 24, p. 100395, 2020.

[22] M. Sumner, B. Palethorpe, and D. W. Thomas, "Impedance measurement for improved power quality-part 1: the measurement technique," vol. 19, no. 3, pp. 1442–1448, 2004.

[23] T. Roinila, T. Messo, and E. Santi, "MIMO-identification techniques for rapid impedance-based stability assessment of three-phase systems in DQ domain," vol. 33, no. 5, pp. 4015–4022, 2017.

[24] N. Mohammed, T. Kerekes, and M. Ciobotaru, "An Online Event-Based Grid Impedance Estimation Technique Using Grid-Connected Inverters," vol. 36, no. 5, pp. 6106–6117, 2020.
[25] S. Cobreces, E. J. Bueno, D. Pizarro, F. J. Rodriguez, and F. Huerta, "Grid impedance monitoring system for distributed power generation electronic interfaces," vol. 58, no. 9, pp. 3112–3121, 2009.
[26] N. Hoffmann and F. W. Fuchs, "Minimal invasive equivalent grid impedance estimation in inductive–resistive power networks using extended Kalman filter," vol. 29, no. 2, pp. 631–641, 2013.
[27] H. J. Tan, S. C. Chan, J. Q. Lin, and X. Sun, "A new variable forgetting factor-based bias-compensated RLS algorithm for identification of FIR systems with input noise and its hardware implementation," vol. 67, no. 1, pp. 198–211, 2019.
[28] C. Paleologu, J. Benesty, and S. Ciochina, "A robust variable forgetting factor recursive least-squares algorithm for system identification," *IEEE Trans. Signal Process.*, vol. 15, pp. 597–600, 2008.
[29] M. Ciobotaru, R. Teodorescu, and F. Blaabjerg, "A new single-phase PLL structure based on second order generalized integrator," in *2006 37th IEEE Power Electronics Specialists Conference*. IEEE, 2006, pp. 1–6.
[30] J. Zhou, S. Kim, H. Zhang, Q. Sun, and R. Han, "Consensus-based distributed control for accurate reactive, harmonic, and imbalance power sharing in microgrids," vol. 9, no. 4, pp. 2453–2467, 2016.

Nabil Mohammed (Member, IEEE) received the bachelor's degree (Hons.) in electrical power engineering from Tishreen University, Latakia, Syria, in 2013, and the M.Eng. degree in electrical engineering from Universiti Teknologi Malaysia, Johor Bahru, Malaysia, in 2017, and the Ph.D. degree in power electronics from Macquarie University, Sydney, Australia, in 2022. During the summer of 2019, he was a Visiting Researcher at the Department of Energy Technology, Aalborg University, Denmark. He is currently a Postdoctoral Research Fellow at Monash University, Australia.
His research interests include power electronics converters, renewable energy generation and integration in power systems, microgrids, energy storage and management systems, and modeling and control of electric systems.

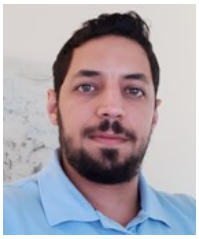

Abderezak Lashab (S'13) received the bachelors and masters degrees in electrical engineering in 2010 and 2012, respectively, from Université des Frères Mentouri Constantine 1, Constantine, Algeria. He received the Ph.D. degree on power electornics in 2019 from Aalborg University, Denmark. He is currently a Postdoctoral Researcher with the same university. From the year 2013 to 2014, he served as an engineer in High Tech Systems (HTS). From 2014 to 2016, he was a Lecturer Assistant in the Université des Frères Mentouri Constantine 1, where he helped in teaching several electrical engineering courses for undergraduate students. He was a Visiting Researcher at the Chair of Power Electronics, Kiel University, Germany from April to July 2019.
His current research interests include power electronics topologies, modeling, and control for photovoltaic systems with and without storage.

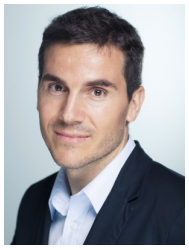

Mihai Ciobotaru (Senior Member, IEEE) received the Eng. Diploma degree and M.Eng. degree in electrical engineering, in 2002 and 2003, respectively, from University of Galati, Galati, Romania. He received the Ph.D. degree in electrical engineering, in 2009, from Aalborg University, Aalborg, Denmark. He continued with the University of Galati as an Associate Lecturer until 2004 and with Aalborg University as an Associate Research Fellow until 2010. He joined the University of New South Wales, Sydney, NSW, Australia as a Research Fellow, where he continued as a Senior Research Fellow until 2018. Thereafter, he joined Macquarie University, Sydney, NSW, Australia, as a Senior Lecturer with the School of Engineering. He is currently an Adjunct Fellow with the Macquarie University, and a Principal Engineer at EcoJoule Energy.
His main research activities and interests include power electronic inverters, power management of hybrid energy storage systems, module-level power electronics for photovoltaic systems, and dc distribution networks for more electric aircrafts.

JOSEP M. GUERRERO (Fellow, IEEE) received the B.Sc. degree in telecommunications engineering, the M.Sc. degree in electronics engineering, and the Ph.D. degree in power electronics from the Technical University of Catalonia, Barcelona, Spain, in 1997, 2000, and 2003, respectively.,Since 2011, he has been a Full Professor with the Department of Energy Technology, Aalborg University, Aalborg, Denmark, where he is responsible for the Microgrid Research Program.
His research interests include power electronics, distributed energy-storage systems, hierarchical and cooperative control, energy management systems, smart metering, and the Internet of Things for ac/dc microgrid clusters and islanded microgrids; recently, there has been a special focus on maritime microgrids for electrical ships, vessels, ferries, and seaports.,Dr. Guerrero is an Associate Editor of the IEEE Transactions on Power Electronics, IEEE Transactions on Industrial Electronics, and IEEE Industrial Electronics Magazine, and an Editor of the IEEE Transactions on Smart Grid and IEEE Transactions on Energy Conversion.